Scientific Research Publishing

Energy and Power Engineering, 2022, 14, 719-736
https://www.scirp.org/journal/epe
ISSN Online: 1947-3818
ISSN Print: 1949-243X

Heat and Mass Transfer by Natural Convection during Transpiration trough a Porous Plate

Abderraouf Sabri[1], Mohamed Asbik[2]

[1]Faculty of Management of Sciences, Universiapolis, Agadir, Morocco
[2]Thermal and Energy Research Team (ERTE), ENSAM, Mohammed V University, Rabat, Morocco
Email: sabri.abderraouf@isiam.ma, mohamed.asbik@ensam.um5.ac.ma

How to cite this paper: Sabri, A. and Asbik, M. (2022) Heat and Mass Transfer by Natural Convection during Transpiration trough a Porous Plate. *Energy and Power Engineering*, **14**, 719-736.
https://doi.org/10.4236/epe.2022.1412039

Received: October 24, 2022
Accepted: December 18, 2022
Published: December 21, 2022

Abstract

Cooling by evaporation through transpiring porous walls is expanding in various industrial applications such as air conditioning. It is also used to cool water in a clay jug. This process deserves to be studied, understood and valued. This paper deals with the transpiration phenomenon through a saturated porous plate coupled with heat and mass transfer by natural convection. Conservation Equations (mass, momentum, energy and concentration), associated with adequate boundary conditions, have been numerically solved using an implicit finite difference iterative method. The numerical model has been validated by experimental measurements from holographic interferometry. The used method to obtain temperature and concentration profiles was explained. They are evaluated from the refractive index of moisture air in the boundary layer. The main numerical results presented are: Nusselt and Sherwood numbers, temperature, humidity, and velocity profiles within the boundary layer as well as the different heat fluxes exchanged between the plate and the surrounding environment. Besides, the present model allows showing the important effect of the equivalent thermal conductivity and the surface emissivity on temperature and heats flux.

Keywords

Transpiration, Natural Convection, Conduction Convection Coupling, Surface Radiation, Holographic Interferometry

1. Introduction

Convective evaporation in porous media occurs in several industrial applications such as industrial refrigeration, cooling of electronics components [1] [2], the energy efficiency of buildings [3], filtration and distillation process of saline water as well as other energy applications [4] [5]. Research carried out in this con-

text allows for optimizing systems and controlling energy expenditure in the field of air conditioning and evaporative cooling by an accurate assessment of heat and mass exchanges between the considered system and the ambient environment.

A review of the literature reveals that this field has been the subject of several research works. Indeed, Mori *et al.* [6] analyzed the theoretical cooling of a porous flat plate by evaporation of a volatile liquid from the surface to a laminar boundary layer flow past it. In this study, the authors considered the effect of injection caused by the vaporization, and also that of 2D thermal conduction in the plate, on the heat and mass transfer characteristics. A comparison of the results of air/methanol and air/water was conducted, and it shows that in the first case, (air/methanol) injection effect is more significant. Jang *et al.* [7] examined numerically mixed convection heat transfer through film evaporation in inclined square ducts. This work was mainly focused on the effects of latent heat of vaporization on the heat transfer improvement, and it has been concluded that the heat transfer rate increases tremendously with phase change. But increasing the relative humidity of moist air in the ambient generates a heat transfer rate decrease. Mechergui *et al.* [8] realized a numerical study coupling heat and mass transfer by natural convection, during water evaporation in a vertical or inclined channel asymmetrically heated with a uniform flux. Conservation Equations (mass, momentum, energy and species) associated with their initial and boundary conditions were numerically discretized using the finite volume method and then solved by the projection method. The numerical results of heat and mass transfer (axial velocity, Nusselt and Sherwood numbers…) are presented.

Besides, great efforts have been made to assess the porous materials which can be used on building roofs to reduce the heat flux that crosses them. Shokri Kuehni *et al.* [3] performed a series of experiments to quantify the performance of an evaporative layer of porous media and highlight the effects of its particle size on decreasing the roof surface temperature. These experimental tests were carried out using three samples of sand, and obtained results showed that porous media with finer (very small particles) texture are more adequate for this application (building energy efficiency). This can be explained by the fact that as particle size decreased the roof surface is kept wet for a long time because the capillary flow connects humid zones and drying ones. In 2017, Nasr *et al.* [9] analyzed numerically free convection for the evaporation of falling pure water film, on one of the plates of a vertical channel. In this study, heat and mass transfers were coupled, and the gas mixture is composed of dry air and water vapor. The wetted plate is coated by a thin porous layer and uniformly heated while the second one is dry and isothermal. It has been shown that the porous layer contributes to improving heat and mass transfer performances at the liquid/gas interface. More recently, an experimental study of heat and mass transfer with phase change in porous media (copper foam) has been presented by Boubaker *et al.* [10]. The main purpose of this work is to highlight the effect of porosity on the heat and mass transfers inside the porous medium. Results revealed that the porosity and aver-

age pore diameter have a significant influence on the phase change within the porous medium and hence their optimal values allow for enhancing thermal performances of the capillary evaporator considered in their study.

Another important aspect of evaporation on a surface is to take into account the effect of thermal radiation on the phase change. Thus, Debbissi *et al.* [4] performed a numerical study that allows the coupling of heat and mass transfers during water evaporation in a vertical channel, under free convection, which is subjected to symmetrical and uniform heat density. Moreover, they also considered radiative heat transfer between the plates. Temperature, velocity and moisture profiles were presented and the effects of various parameters (ambient conditions, wall radiations, …) on heat and mass transfers are depicted. The resulting analysis shows that interfacial heat and mass transfer on the wet plate are dominated by the vaporization of water. However, convection near the dry wall plays an important role in the heat transfer process. Plates with high emissivity increase the amount of water evaporated which means that the optimal case of evaporation occurs when the channel surfaces are considered as a black body. Hossain *et al.* [11] examined numerically the influence of thermal radiation on free convection flow along a vertical semi-finite porous plate uniformly heated with a constant rate of suction. The working fluid has variable dynamic viscosity, Prandtl number Pr = 1, and it is also assumed to be a gray, emitting and absorbing, but non-scattering medium. In addition, the radiative heat flux was estimated using the Rosseland approximation. The governing equations of a proposed mathematical were numerically solved using three different methods. It was concluded that the radiation viscosity parameters have a significant effect on the local skin friction coefficient and the local Nusselt number for different local suction parameters. In 2012, the effect of thermal radiation on 2D steady-state laminar free convection of transparent incompressible fluid along a vertical flat plate has been studied by Sabri *et al.* [12]. They numerically solved heat transfer equations, and showed the effect of surface radiative flux on the characteristics of heat and mass transfers (velocity, temperature and heat flux density). The existence of a threshold value of the thermal resistance, for which average variations of surface temperature are significant, was proven. As for average variations of fluid density, it takes a constant value depending strongly on the emissivity of the plate. Furthermore, increasing the surface emissivity provokes a slight decrease in convective heat flux density while radiative heat flux density increases.

This literature review shows that several research studies have dealt with evaporation in a porous medium by focusing on the flow conditions of evaporated liquids. Nevertheless, research investigations regarding the effect of radiative properties of porous media on convective evaporation are rare.

This paper reports a numerical study of the evaporation of saturated water, by free convection coupled with thermal conduction, inside a vertical (or slightly sloping) porous plate. Additionally, it should be noted that natural convection is driven by thermal and mass buoyancy forces; and the proposed model is validated by experimental measurements. Its originality lies in highlighting how surface

radiation influences heat and mass transfers between the system and its environment. Besides, the effects of different parameters such as ambient humidity, thermal resistance and surface emissivity, on these transfers were revealed too.

2. Mathematical Formulation

2.1. System Configuration

A vertical (or slightly sloping) porous plate of height L and thickness E is considered in this study and the system of coordinates is sketched in Figure 1. The surrounding environment has a temperature (t_a) and a relative humidity (W_a) which are uniform. The back surface of the plate is maintained at the given temperature t_e whereas the front one is saturated with moisture. The plate is sufficiently wide that transverse transfers due to edge effects are neglected.

2.2. Hypotheses

Heat and mass conservation equations are subject to the following assumptions:

- The flow is steady-state, laminar free convection and two dimensional;
- The fluid properties are assumed to be constant except the density variation which is given by Boussinesq approximation in the momentum equation;
- The pressure gradient and the viscous energy dissipation are negligible;
- The fluid is transparent to thermal radiation;
- The longitudinal conduction in the plate is neglected as shown by Miyamoto *et al.* [13] in the case of the imposed temperature.

2.3. Dimensionless Equations

Based on the previous assumptions, the dimensionless equations governing the conservation of mass, momentum, energy and concentration are:

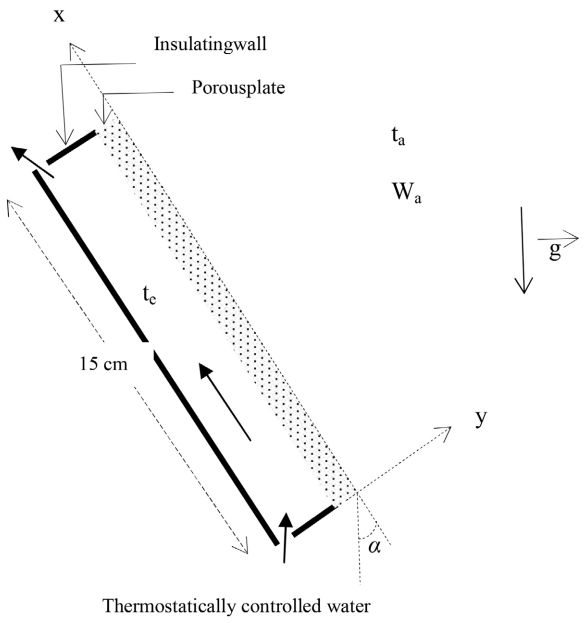

Figure 1. Flow configuration and coordinate system.

$$\frac{\partial U}{\partial X}+\frac{\partial V}{\partial Y}=0 \tag{1}$$

$$U\frac{\partial U}{\partial X}+V\frac{\partial U}{\partial Y}=\frac{\partial^2 U}{\partial Y^2}+T+NA\cdot C \tag{2}$$

$$U\frac{\partial T}{\partial X}+V\frac{\partial T}{\partial Y}=\frac{1}{\mathrm{Pr}}\frac{\partial^2 T}{\partial Y^2}+Q\frac{\partial T}{\partial Y}\frac{\partial C}{\partial Y} \tag{3}$$

$$U\frac{\partial C}{\partial X}+V\frac{\partial C}{\partial Y}=\frac{1}{Sc}\frac{\partial^2 C}{\partial Y^2} \tag{4}$$

where

$$X=\frac{x}{L};\quad Y=\frac{y}{L}Gr_L^{1/4};\quad C=\frac{c-c_a}{c_e-c_a}; \tag{5a-c}$$

$$T=\frac{t-t_a}{t_e-t_a};\quad U=\frac{uL}{\upsilon}Gr_L^{-1/2};\quad V=\frac{vL}{\upsilon}Gr_L^{-1/4} \tag{6a-c}$$

Thermal expansion and concentration expansion coefficients are respectively:

$$\beta_t=-\frac{1}{\rho}\left(\frac{\partial\rho}{\partial T}\right)_{P,C};\quad \beta_c=-\frac{1}{\rho}\left(\frac{\partial\rho}{\partial C}\right)_{T,P} \tag{7a-b}$$

Dimensionless numbers that appear in Equations (2) to (4) are defined as follows:

$$Gr_L=\frac{\beta_t L^3\left(t_e-t_a\right)g\cos\alpha}{\upsilon^2};\quad Pr=\frac{\upsilon}{K};\quad Sc=\frac{\upsilon}{D} \tag{8a-c}$$

$$NA=\frac{\beta_c\left(c_e-c_a\right)}{\beta_t\left(t_e-t_a\right)};\quad Q=\frac{1}{Sc}\frac{C_{P_v}-C_{P_a}}{C_P}\left(c_e-c_a\right) \tag{9a-b}$$

Heat and mass transfers are quantified by dimensionless numbers namely, classical Nusselt number, radiative Nusselt number and Sherwood number. Their local quantities are respectively defined below:

$$Nu\left(x\right)=\frac{q_c\cdot x}{\lambda_f\left(t_s-t_a\right)}=\frac{-1}{t_s-t_a}\left.\frac{\partial t}{\partial y}\right|_{y=0}\cdot x \tag{10a}$$

$$Nu_{rad}\left(x\right)=\frac{q_r\cdot x}{\lambda_f\left(t_s-t_a\right)}=\frac{\varepsilon_s\sigma\left(t_s^4-t_a^4\right)\cdot x}{\lambda_f\left(t_s-t_a\right)} \tag{10b}$$

$$Sh\left(x\right)=\frac{-1}{c_s-c_a}\left.\frac{\partial c}{\partial y}\right|_{Y=0}\cdot x \tag{10c}$$

2.4. Dimensionless Boundary Conditions

The boundary conditions are given in dimensionless form. Thus,

- At the wall, $Y=0$ and $0\le X\le 1$:

$$U=0 \tag{11a}$$

$$V=-\frac{1}{Sc}\frac{C_e-C_a}{1-C_e}\left.\frac{\partial C}{\partial Y}\right|_{Y=0} \tag{11b}$$

$$C=C_s\left(T_s\right) \tag{11c}$$

$$A\left.\frac{\partial T}{\partial Y}\right|_{Y=0}+F\left.\frac{\partial C}{\partial Y}\right|_{Y=0}-B\left(\left(T_s+T_{ar}\right)^4-T_{ar}^4\right)-T_s+1=0 \tag{11d}$$

- $X=0$ and $Y\neq 0$

$$U=0;\ T=0;\ C=0 \tag{12a-c}$$

- $0\le X\le 1$ and $Y\to\infty$

$$U=0;\ T=0;\ C=0 \tag{13a-c}$$

$$T_s=\frac{t_s-t_a}{t_e-t_a};\ T_{ar}=\frac{t_a}{t_e-t_a};\ A=\frac{\lambda_f}{\lambda_s}\frac{E}{L}Gr_L^{1/4} \tag{14a-c}$$

$$B=\frac{\varepsilon_s\sigma}{\lambda_s}E\left(T_e-T_a\right)^3;\ F=\frac{\rho Dh}{\lambda_s}\frac{E}{L}\frac{c_e-c_a}{t_e-t_a}Gr_L^{1/4} \tag{14d-e}$$

The fact that the porous plate is saturated with water and ($t_e - t_a$) < 25˚C (temperature difference not excessive) implies that the effective thermal conductivity is constant [12] [13] and also the temperature profile is linear in it:

$$T=\left(T_s-T_e\right)\frac{L}{E}Gr_L^{-1/4}Y+T_s \tag{15}$$

3. Numerical Analysis

Dimensionless Equations (1) to (4) and boundary conditions (11) to (13) were numerically examined using a fully implicit difference method [14] [15]. These equations were discretized on rectangular mesh chosen to be uniform in each direction, with constant steps Δx_i and Δy_j. Axial convection terms were approached by the upwind scheme whereas the diffusion term was treated with second-order central difference one. Besides, nonlinear terms of these equations were linearized using Newton method. The calculation were carried out at the node "$i+1$" and coupling terms "T and $NA.C$" were evaluated at "i". The velocity V was computed from the continuity equation in order to be injected in the momentum, energy and concentration equations. Obtained algebraic systems of equations were solved using the Thomas algorithm. An iterative procedure has been performed to make necessary corrections to velocities, temperature and concentration values.

On the other hand, Equation (11d) was employed to compute iteratively surface temperature, and convergence is reached when the following criterion is satisfied:

$$\int_0^1\left|\Delta T_s\left(X\right)\right|\cdot \mathrm{d}X\le 10^{-5} \tag{16}$$

Physical properties of humid air [16] were calculated for temperature and humidity values of reference condition (t_r, c_r). Lin *et al.* [17] suggested that the contribution of surface and ambient conditions are respectively 2/3 and 1/3. This suggestion is accepted in this paper and we also assume that:

$$t_s\simeq t_e\ \text{ and }\ c_s\simeq c_e \tag{17a-b}$$

So,

$$t_r = t_e - \frac{1}{3}(t_e - t_a) \tag{18a}$$

$$c_r = c_e - \frac{1}{3}(c_e - c_a) \tag{18b}$$

4. Experimental Study

4.1. Experimental Model Description

Figure 1 shows the scheme of the 2D physical model. It consists of a rectangular parallelepiped form (enclosure) having a porous face made of a thin terracotta plate with a thickness of 8 mm in the first experimental test. In another test we've used a plate of Volvic Lava with a thickness of 2 cm and in both tests, a height of 15 cm, and a width of 40 cm. The enclosure, made from copper, has been insulated with polystyrene and two holes were drilled through lower and upper faces to allow thermostated water circulating. At both sides of the porous plate, the fluid was at temperature t_a and t_e respectively. A LAUDA type thermostat was used to keep the water temperature constant. This should not be high to ensure the saturation condition and to keep water in its liquid state at the plate outer surface.

4.2. Instrumentation and Measurements

The holographic interferometry method has been chosen to perform temperature measurements because of the imposed temperature ranges (t_e around ambient temperature). Furthermore, a classical interferometer (Mach-Zehnder type) has been utilized to experimentally quantifying the index of refraction in a transparent medium [18]. This instrument was associated with a data acquisition system to record and analyze the obtained interferograms as shown in Figure 2, for example.

Interferogram analysis is done at a horizontal straight line. Thus, the first curve gives the light intensity in the form of a frequency-modulated sine wave corresponding to the succession of bright and dark fringes (Figure 3).

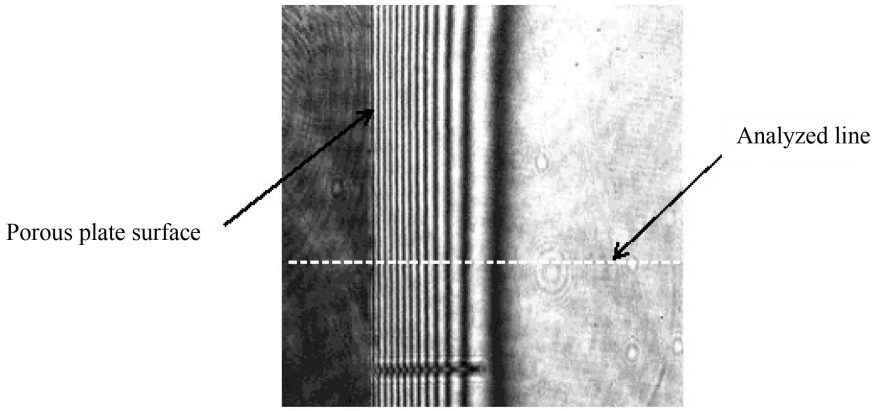

Figure 2. Interferogram to be analyzed.

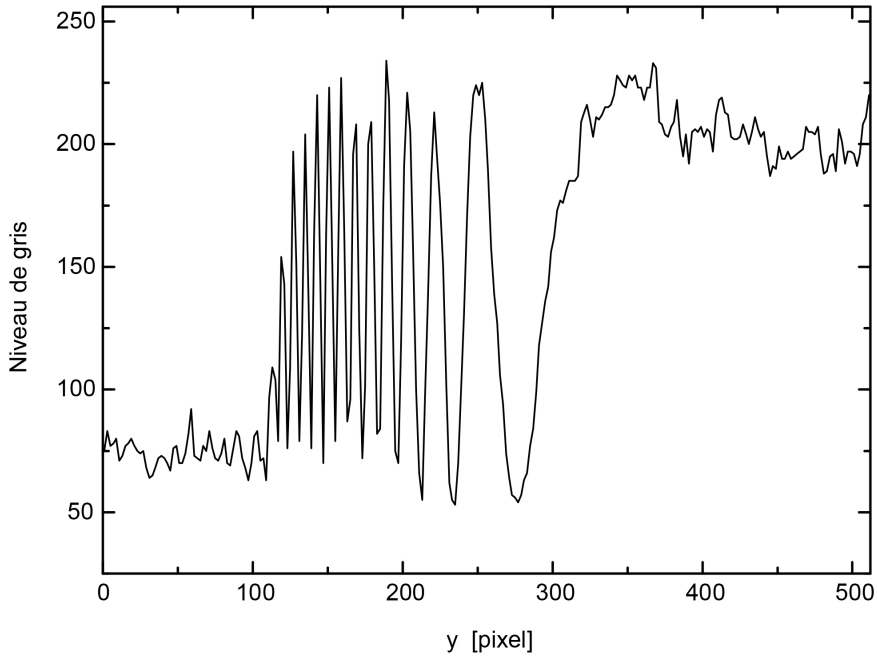

Figure 3. Intensity curve.

Applying a filter to the Fast Fourier Transform (FFT) of the intensity spectrum eliminate undesirable frequencies corresponding to the speckle. Then, the filtered intensity, which corresponds to the real part of the complex signal, was obtained using the inverse fast Fourier transform. The phase which depends on the variation of the index of refraction could be directly computed from the real part and the imaginary part of the complex signals [19]. As a result, **Figure 4** exhibits the profile of the refractive index in the boundary layer on the surface of the previously defined line (see **Figure 2**).

According to the reference [20], the refractive index is a single equation with two unknown variables, namely temperature and humidity which are to be determined. To overcome this difficult, an original approach has been used for their evaluation. Indeed, this approach is based on the similarity between Equations (3) and (4) by assuming that the enthalpy diffusion is not predominant and also the two dimensionless numbers (Pr and Sc) have almost the same value in the case of the water vapor. The induced error remains within the range of the experimental error (1/10) for the interfering distance in the interferogram.

At the surface of the plate, the saturated vapor pressure depends only on the temperature, which is given by Bertrand's law also called Dupré's formula:

$$f_s = 760.10^{\left[17.443-\frac{2795}{t_s}-3.868\log_{10}(t_s)\right]} \tag{19}$$

t_s and f_s are respectively expressed in K and Torr.

In 1967, OWENS [20] conducted a detailed theoretical study based on the formula of LORENTZ-LORENTZ and also on precise experimental measurements carried out using the laser. In its study, he considered air to be a mixture

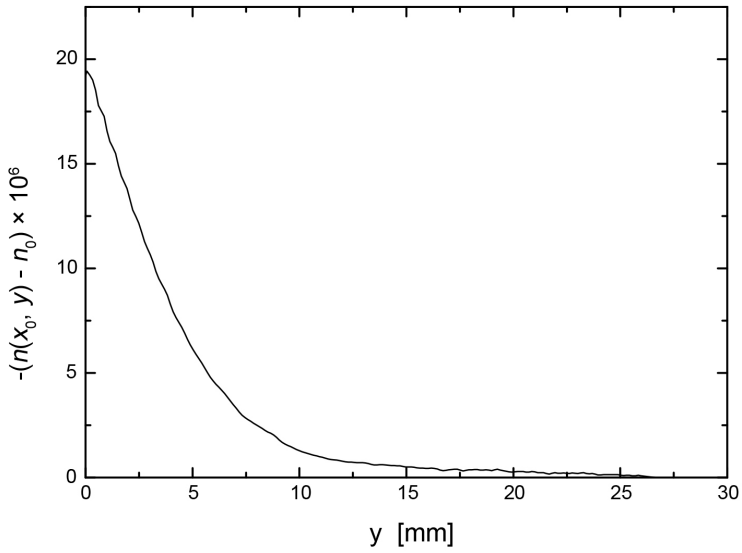

Figure 4. Profile of the refractive index.

of dry air with 0.03% of CO_2, water vapor and carbon dioxide. It resulted in a formula which expresses the refractive index with a precision of 10^{-9} for temperature, pressure relative humidity and wavelength visible radiation values belonging to the following intervals [−23˚C, 47˚C], [0, 4 atm], [0%, 100%] and [3650 Å, 6328 Å] respectively.

$$(n-1)10^8 = K1\left(\frac{P}{720.775}\right)\left[\frac{1+P\left(0.817-0.0133\left(t-273.15\right)\right)10^{-6}}{1+0.003661\left(t-273.15\right)}\right]-K2\cdot f \quad (20a)$$

$$K1 = 8342.13+\frac{2406030}{130-\omega^2}+\frac{15997}{38.9-\omega^2} \quad (20b)$$

$$K2 = 5.722-0.0457\omega^2 \quad (20c)$$

$$\omega = 1/\lambda_L$$

λ_L is the laser wavelength (in μm);

P is the total pressure (in Torr);

f is the vapor partial pressure (in Torr) which can be expressed in term of mass concentration:

$$f = \frac{P\cdot c}{0.622+0.378c} \quad (21)$$

The experimental measurements by holographic interferometry provide the deviation (Δn) of the refractive index from that of the ambient atmosphere. Ambient temperature and humidity will be measured and n_a too. Thus, the equation to be solved is:

$$\Delta n_s + n_a - K1\left(\frac{P}{720.775}\right)\left[\frac{1+P\left(0.817-0,0133\left(t_s-273.15\right)\right)10^{-6}}{1+0.003661\left(t_s-273.15\right)}\right] + K2\cdot 760.10^{\left[17.443-\frac{2795}{t_s}-3.868\log_{10}\left(t_s\right)\right]} = 0 \quad (22)$$

This equation was solved using Newton's iterative method [14] [15] to obtain the surface temperature at the analyzed line and the corresponding saturation concentration is also deduced. Besides, the equality of temperature and concentration dimensionless profiles leads to the following results:

$$c = \left(c_s - c_a\right)\frac{t - t_a}{t_s - t_a} + c_a \tag{23}$$

In the boundary layer, equation to be solved becomes:

$$\Delta n_s + n_a - K1\left(\frac{P}{720.775}\right)\left[\frac{1 + P\left(0.817 - 0.0133\left(t - 273.15\right)\right)10^{-6}}{1 + 0.003661\left(t - 273.15\right)}\right] + K2\frac{P\left[\left(c_s - c_a\right)\frac{t - t_a}{t_s - t_a} + c_a\right]}{0.622 + 0.378\left[\left(c_s - c_a\right)\frac{t - t_a}{t_s - t_a} + c_a\right]} = 0 \tag{24}$$

The same algorithm described above was used to solve this equation. The procedure consists in giving an arbitrary solution at the beginning of each calculation plane. It was taken equal to the exact solution of the neighboring point. This choice is astute because the temperatures between two neighboring nodes are close to one another. As a result, convergence towards the final solution is thus assured and fast and hence temperature and humidity profiles are respectively obtained.

4.3. Validation of the Numerical Method

In the case of the Volvic, lava plate which has a thermal resistance with an equivalent conductivity λ_s; **Figure 5(a)** and **Figure 5(b)** show the temperature and humidity profiles at a distance x_0 from the bottom edge of the plate, and under the physical conditions listed below.

In another experimental test, a thin terracotta plate was used. It has a low thermal resistance which allows having an isothermal surface. This result, considered as a hypothesis of numerical simulation, was confirmed by temperature measurements using thermocouples. **Figure 6(a)** and **Figure 6(b)** show the fitted experimental profiles for which uncertainties were considered. The uncertainty calculation was developed based on the error of 1/10 of the interfringe in the interferogram. This allows us to estimate Δt and Δc mentioned in **Figure 6(a)** and **Figure 6(b)**. It clearly appears that the theoretically calculated temperature profiles are ranging within the experimental uncertainty interval and the relative deviation does not exceed 5%. Additionally, it is obvious that there is a net difference between the theoretical and experimental concentration profiles, especially inside the boundary layer. This is due to the experimental measurement method proposed above, which is based on the similarity of dimensionless temperature and concentration profiles. Nevertheless, the deviation is less than 20% in the worst case.

To the best of our best knowledge, it is important to point out that there are no similar results to which this work could be compared.

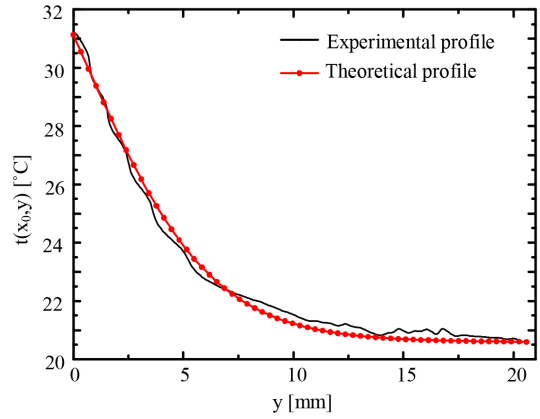

(a)

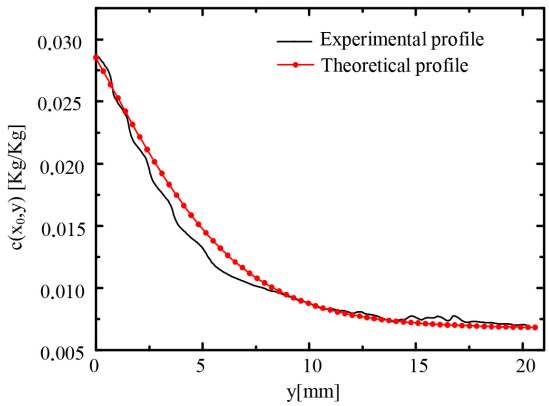

(b)

Figure 5. Comparison between measurement values and theoretical temperature and concentration profiles. $E = 2$ cm; $L = 15$ cm; $x_0 = 4$ cm; $\alpha = 33^\circ$; $\lambda_s = 0.56$ W/m˚C; $\varepsilon_s = 0.9$; $t_a = 20.6^\circ$C; $W_a = 45\%$; $t_e = 43.4^\circ$C.

5. Results and Discussion

5.1. Thermal Behavior of Porous Plate Surface

In this study, the following parameters have generally constant values:

Pr	Sc	Gr_L	NA	Q	A	F	L (cm)	E/λ_s (m^2·K/W)	W_a (%)	t_e (K)	t_a (K)
0.703	0.591	6.048×10^6	0.502	0.058	0.893	6.789	15	0.01	30%	313.15	298.15

And $B = 0 \rightarrow 1.913 \times 10^{-6}$.

The surface is assumed to be gray and it is characterized by a constant emissivity ε_s. According to the surface temperature, the porous plate can emit or absorb the radiative energy. Figure 7 and Figure 8 show the evolution of the temperature and the heat flux density at the surface with respect to different emissivity values. It is observed that the increase of ε_s favors the temperature drop (Figure 7) and hence the hence the heat evacuation (Figure 8). In the same conditions, the thermal radiation emitted at the surface is exhibited in Figure 9.

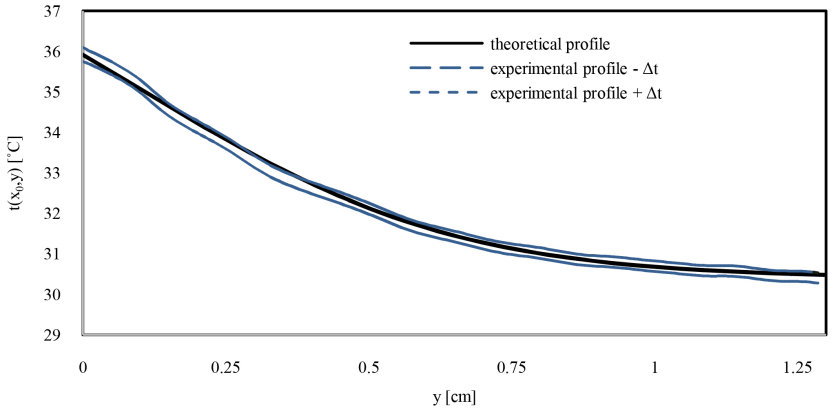

(a)

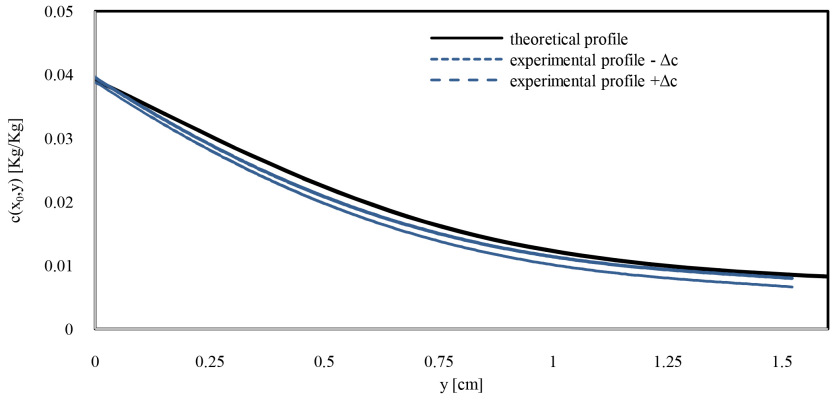

(b)

Figure 6. (a): Comparison between measurement values and theoretical temperature. x_0 = 4 cm; $\alpha = 0^\circ$; W_a = 24.7%; t_s = 35.9˚C; (b): Comparison between measurement values and theoretical concentration. x_0 = 4 cm; $\alpha = 0^\circ$; W_a = 24.7%; t_s = 35.9˚C.

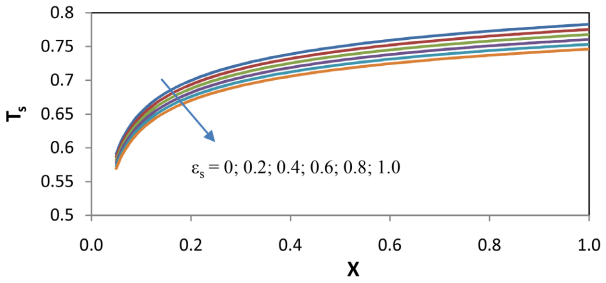

Figure 7. Emissivity effect on the surface temperature.

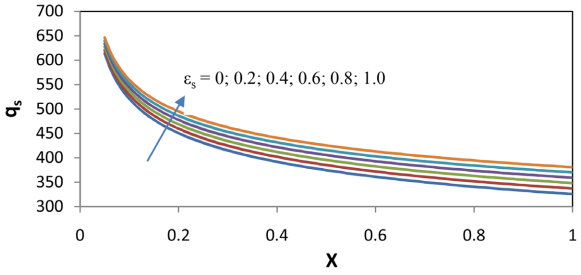

Figure 8. Emissivity effect on the heat flux density through the porous medium.

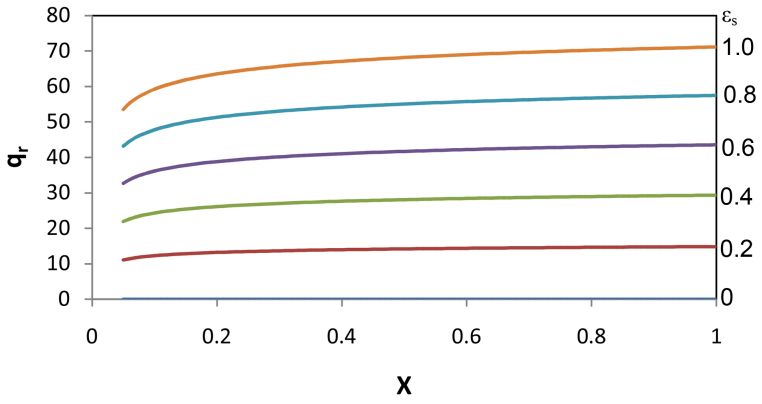

Figure 9. Emissivity effect on the radiative flux density at the surface.

The ambient relative humidity, W_a, is a very influential factor on the heat and mass exchanges between the porous plate and the external environment. Thus, **Figure 10** depicts average heat density versus W_a for various emissivity values. These curves linearly decrease with relative humidity and they undergo a drop from 35% to 39%. As for the density $<q_s>$, it increases by 10% to 20% if the emissivity goes from 0 to 1.

5.2. Heat and Mass Transfer

Heat and mass transfer are evaluated in the following conditions (**Figures 11-15**):

Pr	*Sc*	Gr_L	*NA*	*Q*	*L* (cm)	W_a	t_e (K)	t_a (K)
0.706	0.598	2.213×10^6	0.680	2.642×10^{-2}	15	40%	303.15	298.15

And $A = 6.808 \times 10^{-4} \rightarrow 1.362$, $B = 0 \rightarrow 1.418 \times 10^{-7}$, $F = 7.157 \times 10^{-3} \rightarrow 14.313$.

The thermal resistance (E/λ_s) for heat conduction through the porous plate is impacting the heat balance at the surface (Equation (5d)), and it also plays an important role by coupling conduction and convection modes of heat transfer. To be sure, **Figure 11** illustrates average dimensionless temperature as a function of this resistance for two extreme values of ε_s (0 and 1). It has been shown that the effect of (E/λ_s) becomes tangible from around the value of 10^{-4} (m^2·K/W). Therefore, the surface is no longer isothermal and its temperature decreases all the more so the evacuated heat radiation from the surface contributes and slightly lowers this temperature. Furthermore, **Figure 12** shows increasing of evacuated heat with the emissivity and in this case, it goes from 16% to 7% if the emissivity varies from 0 to 1. For each ε_s value; it remains constant until a specific thermal resistance value where it starts to decrease.

Figure 13 depicts the variation of the average classical Nusselt number as a function of the plate thermal resistance for different surface emissivity values. A significant growth of this number is seen when the plate is more resistive and becomes more sensitive to the radiation of the surface.

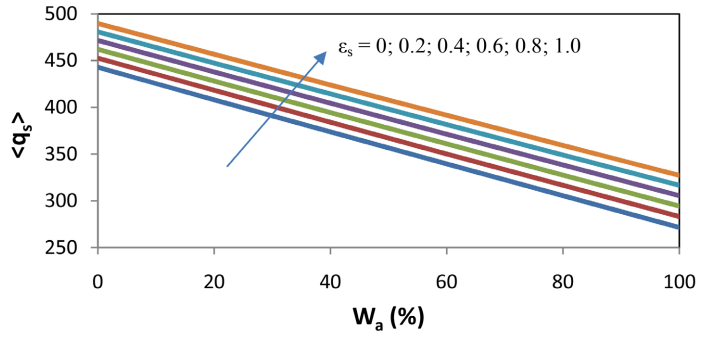

Figure 10. Average heat flux through the porous plate versus the ambient humidity.

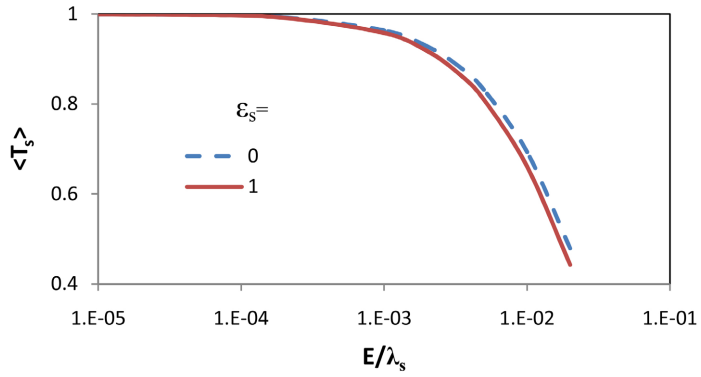

Figure 11. Average dimensionless temperature with respect to thermal resistance.

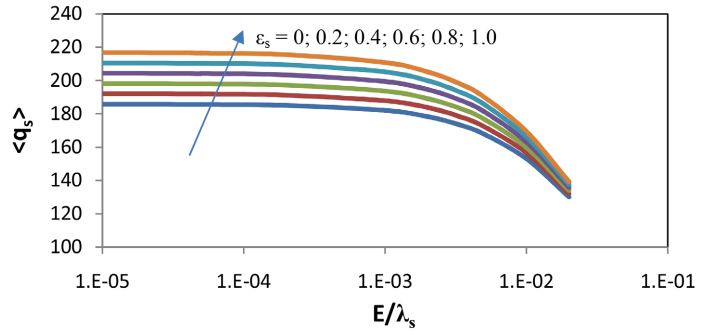

Figure 12. Average heat flux density through the porous plate as a function of thermal resistance.

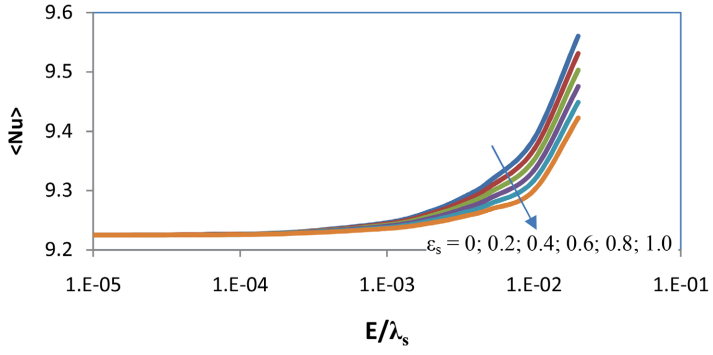

Figure 13. Average classic Nusselt number as a function of thermal resistance.

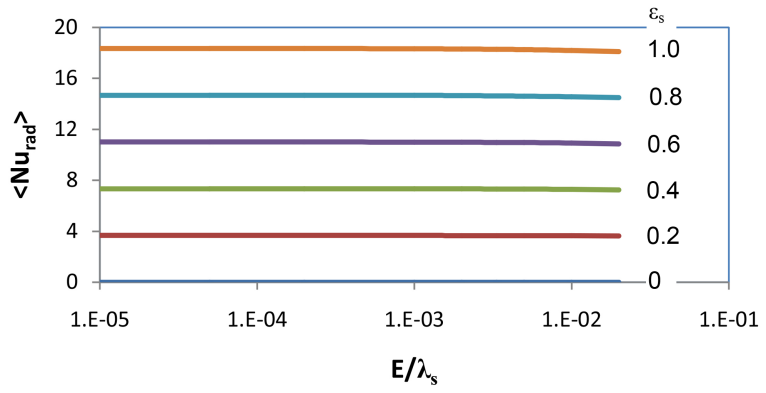

Figure 14. Average radiative Nusselt number as a function of thermal resistance.

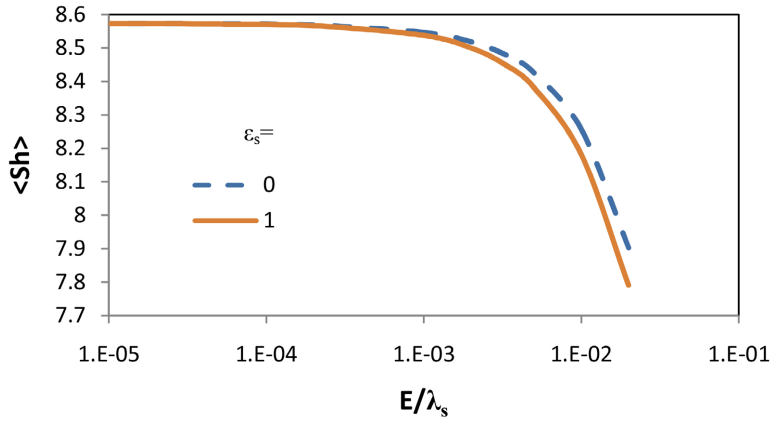

Figure 15. Average classic Sherwood number as a function of thermal resistance.

Figure 14 illustrates the average radiative Nusselt number as a function of the thermal resistance of the plate for different values of surface emissivity. It appears to be insensitive to the thermal resistance of the plate and remains almost constant. However, on the other hand, it varies strongly in a linear manner with the emissivity of the surface.

Figure 15 shows the average Sherwood number as a function of thermal resistance for the extreme cases of the emissivity value. This number decreases rapidly when the plate has more and more thermal resistance, this means that the mass exchange by convection decreases compared to the mass exchange by diffusion when the surface temperature decreases. Note that Sherwood number is also sensitive to the value of emissivity and that the relative difference of this one can go up to 1.5% for the extreme cases of emissivity. This parameter is in the Equation (11d) which expresses the continuity of the heat flux at the surface. This equation contains the latent heat flux which is expressed as a function of the concentration gradient. We know that Sherwood's number depends on it, which leads to the influence of emissivity on this dimensionless magnitude.

To compare involved heat flux, Figure 16 presents their evolution in term of the temperature at the enclosure bottom. Note that the latent heat flux is more important than other heat flux types (sensible and radiative heat fluxes). The

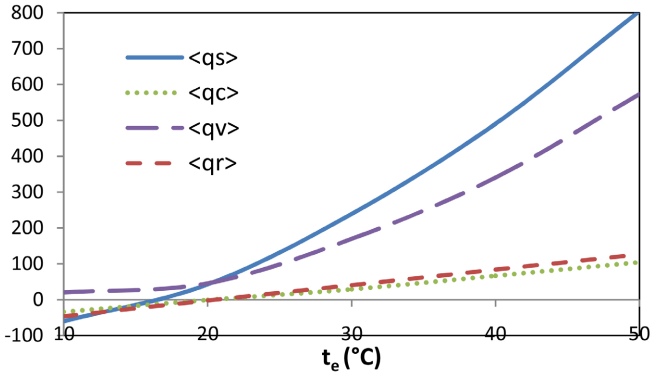

Figure 16. Comparison between various types of average heat fluxes. E/λ_s = 0.01 m²·K/W, ε_s = 0.9, t_a = 293.15 ˚K, W_a = 40%.

latter is close to the sensible heat flux or even greater when the emissivity exceeds 0.8.

For an ambient temperature of 20˚C and a relative humidity of 40%, water temperature has been varied in the chamber from 10˚C to 50˚C to examine conduction heat fluxes at the inlet/exit of the plate.

There is an equilibrium point for which this flow through the plate is null, which is approximately 16˚C for the value of t_e. Regarding the cooling system in the ambient air under the aforementioned conditions, this last value corresponds to the equilibrium temperature of water in the enclosure.

6. Conclusions

The numerical model of the conduction-convection coupling allowed us to calculate the distributions of the Nusselt and Sherwood numbers, temperature, humidity, and velocity profiles within the boundary layer as well as the different heat fluxes exchanged between the plate and the surrounding environment.

The thermal resistance of the plate has an important influence on the transfers. There is a limit to this parameter for which the plate no longer has any resistance, and the surface becomes practically isothermal.

We can conclude that surface radiation, which is one of the modes of heat transfer between the plate and the surrounding environment, plays a very important role in the transpiration process. The heat flux by radiation is always comparable and sometimes more intense than the sensible heat flux for a real range of emissivity of the surface. As the emissivity of the surface increases, the radiative energy sent to the environment increases, which leads to a decrease in the surface temperature and an increase in the conduction flow within the plate.

The present model provides a better understanding of the cooling process by natural evaporation. Water is the evaporated substance in the case of this study, but the model remains valid for any other material with phase change as long as the assumptions made are valid. Highlighting the influence of parameters such as: equivalent thermal resistance and surface emissivity, on this system could contribute to the optimization of the system to reach the desired thermal and mass

exchanges.

During the subsequent study, it would be interesting to take into account the heat and mass transfer in the porous medium to deal with the case of a no-saturated surface in moisture.

Conflicts of Interest

The authors declare no conflicts of interest regarding the publication of this paper.

References

[1] Rosenfeld, J.H. and North, M.T. (1995) Porous Media Heat Exchangers for Cooling of High-Power Optical Components. *Optical Engineering*, **34**, 335-341. https://doi.org/10.1117/12.194100

[2] Zheng, L.J., Kang, D.H., Kim, N.K., Youn, Y.J. and Kang, H.W. (2019) Theoretical Analysis of Natural Evaporative Cooling to Enhance the Efficiency of Thermoelectric Devices. *International Journal of Heat and Mass Transfer*, **143**, Article ID: 118512. https://doi.org/10.1016/j.ijheatmasstransfer.2019.118512

[3] Shokri Kuehni, S.M.S., Bou-Zeid, E., Webb, C. and Shokri, N. (2016) Roof Cooling by Direct Evaporation from a Porous Layer. *Energy and Building*, **127**, 521-528. https://doi.org/10.1016/j.enbuild.2016.06.019

[4] Debbissi, C., Orfi, J. and Ben Nasrallah, S. (2001) Evaporation of Water by Free Convection in Vertical Channel Including Effects of Wall Radiative Properties. *International Journal of Heat and Mass Transfer*, **44**, 811-826. https://doi.org/10.1016/S0017-9310(00)00125-3

[5] Bouddour, A., Auriault, J.-L., Mhamdi-Alaoui, M. and Bloch, J.-F. (1998) Heat and Mass Transfer in Wet Porous Media in Presence of Evaporation-Condensation. *International Journal of Heat and Mass Transfer*, **41**, 2263-2277. https://doi.org/10.1016/S0017-9310(98)00002-7

[6] Mori, S., Kumita, M., Takahashi, T., Tanimoto, A. and Sakakibara, M. (1997) Heat and Mass Transfer from a Flat Plate of Finite Thickness to a Boundary Layer Flow with Transpiration. *Energy Conversion and Management*, **38**, 1209-1218. https://doi.org/10.1016/S0196-8904(96)00150-1

[7] Jiang, J.-H., Yan, W.-M. and Huang, C.C. (2005) Mixed Convection Heat Transfer Enhancement through Film Evaporation in Inclined Square Ducts. *International Journal of Heat and Mass Transfer*, **48**, 2117-2125. https://doi.org/10.1016/j.ijheatmasstransfer.2004.12.022

[8] Mechergui, O., Chesneau, X. and Laatar, A.H. (2017) Heat and Mass Transfers by Natural Convection during Water Evaporation in a Vertical Channel. *Computational Thermal Sciences*: *An International Journal*, **9**, 423-445. https://doi.org/10.1615/ComputThermalScien.2017019798

[9] Nasr, A. and Al-Ghamdi, A.S. (2017) Numerical Study of Evaporation of Falling Liquid Film on One of Two Vertical Plates Covered with a Thin Porous Layer Free Convection. *International Journal of Thermal Sciences*, **112**, 335-344. https://doi.org/10.1016/j.ijthermalsci.2016.10.018

[10] Boubaker, R., Harmand, S. and Platel, V. (2018) Experimental Study of Liquid/Vapor Phase Change in a Porous Media of Two-Phase Heat Transfer Devices. *Applied Thermal Engineering*, **143**, 275-282. https://doi.org/10.1016/j.applthermaleng.2018.07.058

[11] Hossain, M.A., Khanafer, K. and Vafai, K. (2001) The Effect of Radiation on Free

Convection Flow of Fluid with Variable Viscosity from a Porous Vertical Plate. *International Journal of Thermal Sciences*, **40**, 115-124. https://doi.org/10.1016/S1290-0729(00)01200-X

[12] Sabri, A., Asbik, M. and Zeghmati, B. (2012) Effect of the Surface Radiation on the Free Convection Heat Transfer Interacted with Thermal Conduction inside a Vertical Flat Plate. *AMSE Journals*, *Modeling*, *Measurement and Control*, *Serie B*: *Mechanics and Thermics*, **81**, 82-98.

[13] Miyamoto, M., Sumikawa, J., Akiyoshi, T. and Nakamura, T. (1980) Effects of Conduction in a Vertical Flat Plate on Free Convection Heat Transfer. *International Journal Heat and Mass Transfer*, **23**, 1545-1553. https://doi.org/10.1016/0017-9310(80)90158-1

[14] Dale, A.A., Tannehil, J.C. and Pletcher, R.H. (1984) Computational Fluid Mechanics and Heat Transfer. Hemisphere Publishing Corporation, New York.

[15] Gourdin, A. and Boumhrat, M. (1983) Méthodes Numériques Appliquées. TEC&DOC Lavoisier, Paris.

[16] Fujii, T., Kato, Y. and Mihara, K. (1977) Expressions of Transport and Thermodynamic Properties of Air, Steam and Water. *Univ. Kyushu Research Institute of Industrial Science Rep.*, **66**, 81-95. https://cir.nii.ac.jp/crid/1573105975198877568

[17] Lin, T.F., Chang, C.J. and Yan, W.M. (1988) Analysis of Combined Buoyancy Effects of Thermal and Mass Diffusion on Laminar Forced Convection Heat Transfer in a Vertical Tube. *Journal of Heat Transfer*, **110**, 337-344. https://doi.org/10.1115/1.3250489

[18] Vest, C.M. (1980) Holographic Interferometry: Some Recent Developments. *Optical Engineering*, **19**, Article ID: 195654. https://doi.org/10.1117/12.7972584

[19] Kreis, T. (1986) Digital Holographic Interference-Phase Measurement Using the Fourier-Transform Method. *Journal of the Optical Society of America*, **3**, 845-855. https://doi.org/10.1364/JOSAA.3.000847

[20] Owens, J.C. (1967) Optical Refractive Index of Air: Dependence on Pressure, Temperature and Composition. *Applied Optics*, **6**, 51-60.